https://doi.org/10.1016/j.apor.2021.102630

Micro-mechanical analysis of caisson foundation in sand using DEM: particle shape effect

Zhen-Yu YIN[1] and Pei WANG[1,2] *

Affiliations:

[1] Department of Civil and Environmental Engineering, The Hong Kong Polytechnic University, Hung Hom, Kowloon, Hong Kong, China

2 Southern Marine Science and Engineering Guangdong Laboratory (Guangzhou), 1119 Haibin Rd., Nansha District, Guangzhou, China

* Corresponding authors: Dr. Pei WANG, Tel: +852 3400 8470; Fax: +852 2334 6389; Email: peiwang@polyu.edu.hk

Abstract: The caisson foundation has been extensively studied with experimental, analytical and numerical methods. However, the effect of particle shape on the caisson foundation is somehow ignored. In this paper, the caisson foundation is analyzed with DEM and the effect of particle shape is discussed in detail by introducing spherical and tetrahedral particles without rolling resistance, and spherical particle with rolling resistance. Firstly, a series of biaxial tests are simulated on samples with different particle shapes to obtain the soil properties, and typical shear behaviors are observed in all simulations. Then the effect of particle shape on the macro- and microscopic behaviors of caisson foundation is then investigated with different loading conditions. The results show that when subjected to external loading, compared with spherical particles, caisson foundation with angular particles or spherical particles with rolling resistance (1) has increased horizontal and rotational bearing capacities; (2) has much smaller particle rotation due to the strong interlocking capacity between particles; (3) exhibits higher stress concentration and magnitude of force chains; and (4) experiences significant increase on the magnitude of the anisotropy.

Keywords: Caisson foundation; particle shape; micromechanics; microstructure; discrete element method; granular soils

1. Introduction

Caisson foundation has been extensively used for offshore structures such as bridge piers and wind turbines. Caisson foundation is an upside down steel or concrete tube embedded in the seabed. During the installation process, a caisson is usually floated to the job site and sunk into place. And the caisson is push to the final position by the suction force induced by pumping the water out of the caisson. Caisson foundation is often subjected to the loading condition which can be characterized by large overturning moment and small vertical and horizontal loads. Compared with other types of foundations used for offshore structures, it is more cost-effective and environment-friendly.

Caisson foundation has been extensively studied with experimental, analytical and numerical methods. For the experimental aspect, the moment loading capacity, vertical loading response, penetration velocity, seismic behavior, and soil-structure interaction of caisson foundation subjected to monotonic or cyclic loadings were investigated in detail using small-scale model test, centrifuge test or full-scale test (Barari and Ibsen, 2012; Byrne and Houlsby, 2002; Chang et al., 2014; Cox et al., 2014; Jia et al., 2018; Kelly et al., 2006; Kou et al., 2019; Zhu et al., 2011; Zhu et al., 2019). In addition, analytical methods, including strain-hardening plasticity model (Cassidy et al., 2006; Villalobos et al., 2009), macro-element method (Jin et al., 2019c; Skau et al., 2018), upper bond plasticity method (Yun and Bransby, 2007) and hyperplasticity theory (Nguyen-Sy and Houlsby, 2005) were used to study the bearing capacity and failure mechanism of caisson foundation. In terms of the numerical analysis, finite element method (FEM) and finite difference method (FDM) were used to investigate the behaviors of caisson foundation at various working conditions, to validate the experimental results and to reproduce the failure mechanisms provided by analytical methods (Achmus et al., 2013; Bagheri et al., 2017; Jin et al., 2019a; Jin et al., 2019b; Mehravar et al., 2016; Mehravar et al., 2017). Recently, discrete element method (DEM) was used to study the behavior of a caisson foundation during its installation, operation and failure, in which the micro-mechanical analysis of the behaviors of caisson foundation was conducted (Wang and Yin, 2020). The advantage of using DEM to analyze the caisson foundation lies in the fact that it can physically capture the large deformation of soil particles, and thus provide us not only the bearing capacity but also failure mechanisms of caisson foundation. Therefore, in this follow-up study, the effect of particle shape, which is one of the most important characteristics of soil particles, on the micro-mechanical behavior of caisson foundation is investigated.

The seabed soils are usually non-homogeneous and subjected to natural spatial variation in terms of soil behavior and particle micro-structure (Peng et al., 2017; Sui et al., 2019). Therefore, geotechnical survey and soil classification are often conducted before the construction of offshore structures (Thusyanthan, 2012). Previous research showed that the bearing capacity of a caisson foundation is closely related to the soil condition and mechanical properties (!!! INVALID CITATION !!! (Bagheri et al., 2017; Kelly et al., 2006; Yun and Bransby, 2007)). In addition, as proved by many studies, particle shape has a strong influence on soil properties such as strength and frictional angle. For example, the critical state friction angle of sand was reported to decrease markedly with an increase of rounded fine contents in sand (Yang and Wei, 2012). Similar results were also found in (Podczeck and Miah, 1996; Yang and Luo, 2015), which was attributable to the increased interlocking effect among particles (Shinohara et al., 2000). Particle shape also influenced the distribution of stress among particles by propagating force chains more efficiently in rough particle than frictionless systems (Guises et al., 2009). In addition, soil compressibility and dilation are also closely related to particle shape (Afzali-Nejad et al., 2017; Cavarretta et al., 2010; Wang et al., 2019). The effect of particle shape on soil behavior has also been extensively investigated and validated by using the DEM, in which the angularity can be approached by bonding a number of spheres, applying polygon-shaped or egg-shaped particles, and imposing rolling resistance torque to particles (Cui et al., 2020; Gong et al., 2019; Zhou et al., 2018a). In the first two methods, particles have shapes that are physically similar to real soil particles, while the rolling resistance method provides a numerical way to simulate angular particles. In the case of caisson foundation, the increase of soil particle angularity is expected to increase its bearing capacity due to the enhanced interlocking between particles and the improved engineering properties of soils. In addition, the particle shape also has an influence on the size of failure zone during the failure of a caisson foundation. Thus, it is important to account for the effect of particle shape in the analysis of caisson foundation, which, however, has been unfortunately ignored in previous studies.

In this paper, caisson foundation is analyzed with DEM, in which the effect of particle shape is discussed in detail with different load combinations. The particle angularity is achieved by introducing two simple but common particle shapes, i.e. spherical and tetrahedral, which allows the evaluation of the effect of particle shape at the engineering scale with relatively low computation cost. In addition to physically changing the particle shape, the rolling resistance method, which indirectly reproduces the behavior of irregular particles, is also applied. The property of soils is first investigated with a series of biaxial tests using DEM. Then the micromechanical analysis focuses the effect of particle shape on the behavior of caisson foundation.

2. DEM model verification

2.1. Representation of particle shape

Particle shape plays an important role in determining the properties and behaviors of granular materials at both microscale and macroscale (Cho et al., 2006). Various methods have been proposed in DEM to model the angularity of soil particles, such as cluster method, spherical harmonic method and level set method (Fan et al., 2020; Fu et al., 2017; Kawamoto et al., 2016; Zhou et al., 2013). Study in this paper is conducted in 2D, which has benefits of low-cost and ease of visualization. In 2D, these methods can be generally divided into two categories: single particle method and composite method (Zhang et al., 2017). Single particle method includes the circular-shaped and non-circular-shaped particles that are directly implemented in DEM algorithms. The circular-shaped is the most commonly used particle shape in DEM simulation due to its simplicity and computational efficiency. Despite the over-simplified shape, this method has been proved successful in simulating the behavior of soils (Chen et al., 2018; Xiang et al., 2018; Zhou et al., 2018b; Zhou et al., 2019). In order to have more realistic particle shape, non-spherical particles, such as ellipse-shaped, egg-shaped, and polygon-shaped particles, have also been implemented in DEM simulations (Alonso-Marroquin et al., 2008; Ting et al., 1993; Zhou et al., 2018a). In terms of the composite method, arbitrary particles can be represented by connecting a number of elements or spheres (Huang et al., 2020; Yin et al., 2020; Zhao et al., 2020). Depending on the deformability and the strength of the bonds, the composite method can simulate deformable and crushable particles as well as rigid ones (clumps). Another advantage of this method is that contact detection and force calculation are much easier than that of non-circular-shaped particles. However, the number of discs and computation cost increase significantly when the particle shape is complex, which make it not appropriate for engineering scale analysis. In this study, because of the large scale of the caisson foundation model, the spherical particle (SP) from the single particle method and tetrahedral particle (TP) from the composite method are adopted. The clump logic is used in the TP, which makes the particle rigid and unbreakable. The distance between the two sphere centers in TP is 1.2 times of the sphere radius. The SP in DEM is used to simulate rounded or sub-rounded particles in reality, while the TP is used to reproduce the surface roughness of angular particles. It is important to mention that by connecting a large number of spheres, particle with much more realistic shapes can be obtained in DEM simulations. However, the high computational cost makes it not appropriate this study. Therefore, simple shapes with only one and three spheres are used in this study. During the sample preparation, the expansion method, in which the sizes of particles are adjusted by increasing/decreasing the radii of elementary spheres, is used to make sure that different types of particles have same volume. The geometries of the particles are shown in Figure 1(a) and (b). Samples consisting of only single particle shape and two particle shapes are investigated, which are named as S100, T100, S75T25, S50T50 and S25T75 according to the relative fractions of the two shapes.

Because reproducing realistic particle shapes with the clump method in DEM requires a large number of spheres which is usually computationally expensive, an alternative method to indirectly reproduce the behavior of irregular particles, i.e. rolling resistance method, was also adopted in some studies (Jiang et al., 2005; Wensrich and Katterfeld, 2012). The rolling resistance can arise from several sources at the contact between two particles, such as micro-slip at the interface, plastic deformation around the contact, viscous hysteresis, surface adhesion and particle shape effect (Ai et al., 2011). And particle shape is the most important mechanism in the quasi-static analysis of granular materials (Wensrich and Katterfeld, 2012). In DEM, the motion of a particle is described by the rotational velocity and the translational velocity of its centroid. When there is no rolling resistance, particle can rotate without resistance and energy loss, which is not a realistic behavior. Therefore, in the rolling resistance method an artificial rotational torque to account for the rolling resistance is applied to any two connecting particles with a relative rotational increment. The direction of the torque is against the direction of the relative rotational increment and the increment of the resistance torque is expressed as

$$\Delta\mathbf{M}^{\mathbf{r}} = k_r \Delta\boldsymbol{\theta}_{\mathbf{b}} \quad (1)$$

in which $\Delta\mathbf{M}^{\mathbf{r}}$ is the torque increment applied on the particle; k_r is the rolling resistance stiffness; and $\Delta\boldsymbol{\theta}_{\mathbf{b}}$ is the relative rotation increment. The maximum limiting rolling resistance is equal to the product of normal force with a rolling friction coefficient, and effective contact radius, which is expressed as

$$\mathbf{M}^{\mathbf{r}}_{\max} = \mu_r F_n \overline{R} \tag{2}$$

where μ_r is the rolling friction coefficient; F_n is the magnitude of the current normal force; and $\overline{R}$ is the effective contact radius which is given by $1/\overline{R} = 1/R_1 + 1/R_2$ (R_1 and R_2 are the radii of the connecting balls). μ_r ranges from zero to infinity which corresponds to no rolling resistance and very high resistance. Therefore, one of the advantages of this method lies in the fact that it can simulate particles with arbitrary angularity by just changing the friction coefficient. In addition, because each particle only contains one elementary spheres, the computational cost is low. The rolling resistance method has been proved to successfully reproduce the macroscopic behavior of angular particles (Salazar et al., 2015; Yang et al., 2017), and a detailed description of this method is available in (Ai et al., 2011). In this study, the rolling resistance method with the μ_r equal to 0.25, 0.5 and 0.75 is applied to SP to investigate the effect of particle shape, as shown in Figure 1(c).

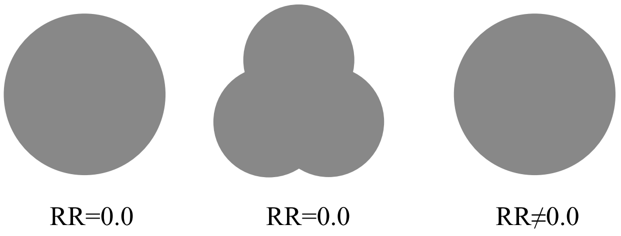

(a) (b) (c)

Figure 1. Representation of particle shapes in DEM simulation: (a) spherical particle (SP) with μ_r =0.0; (b) tetrahedral particle (TP) with μ_r =0.0 and (c) SP with $\mu_r \neq$0.0

2.2. Effect of particle shape on shear behavior

Because the shear behavior of soils has a strong influence on the loading capacity of caisson foundation, a series of biaxial tests are simulated with different particle shapes and rolling resistance to investigate their influences on the shear behavior. The soil used in this study is well-graded sand which has a particle size distribution (PSD) parallel to that of the sand used in the experiments by Foglia *et al.* (2015) and a mean grain size of 2.5 mm which is 18 times higher to avoid high computational cost. Because of this change, the ratio of particle size and specimen size (and later caisson size) is much higher than the reality. However, the validity of the DEM is not impaired by the increased particle size according to the typical macroscopic shear behaviors observed in the biaxial shear tests and reasonable residual friction angles compared with experiments (Rousé et al., 2008; Wu et al., 2017). Both loose and dense sand are prepared with a relative density of 20% and 80%, respectively. The relative density is given by

$$D_{relative} = \frac{e_{\max} - e}{e_{\max} - e_{\min}} \times 100\%. \quad (3)$$

The method proposed by Wood and Maeda (2008) is used to determine the maximum and minimum void ratios ($e_{\max}$ and $e_{\min}$), and to generate samples with different relative densities. Specimens were prepared as follows: (1) four walls forming a box shape with 80 mm in height and 40 mm in width are generated and work as the boundaries of the sample; (2) the number and size of soil particles are obtained based on the PSD and porosity n_g, and then non-overlapped particles are randomly generated within the box; (3) initial particle friction coefficient μ_{ini}^{p} and other micro-mechanical parameters shown in Table 1 are applied; (4) the particle assembly is subjected to an isotropic compressive stress of $\sigma_{m0} = k_n \times 10^{-4}$; (5) the friction coefficient is changed to the final value μ^{p}, and the sample is stabilized to reach a state of equilibrium with σ_{m0}; (6) the final confinement stress of 200 kPa is applied. The sample with $e_{\min}$ is obtained when the μ_{ini}^{p} and n_g are respectively 0.0 and 0.1 (Wood and Maeda, 2008). While the $\mu_{ini}^{p}=1.0$ and $n_g=0.3$ give the loosest sample with $e_{\max}$. For samples with other relative densities, the void ratio e is firstly calculated based on Eq. (3), and then $n_g=e/(1+e)$ and $\mu_{ini}^{p}=0.1$ are respectively adopted in the steps (2) and (3). After the preparation process, the sample is then subjected to a vertical compression while the confinement stress is kept constant in the horizontal direction during the simulation. The vertical compressive stress, vertical displacement and horizontal displacement are monitored throughout the modeling. The particle interactions are governed by the linear contact model in which linear elastic (no-tension) frictional behavior with constant normal and shear stiffness is provided. The values of micro-mechanical parameters used in the DEM simulation are summarized in Table 1. The density of sand particle is 2600 kg/m^{3,} which is a typical value for sand. The normal and shear stiffness of both sand particle and wall are respectively chosen as 1.5×10^{8} N/m and 1.0×10^{8} N/m, which ensures small overlap (less than 2% of average particle diameter) between contacting particles. An empirical value of friction coefficient 0.5 is used for particles according previous studies (Wang and Arson, 2018; Wang et al., 2020; Zhang et al., 2019). And the walls are assumed smooth and have a friction coefficient of 0.0. The rolling friction coefficient is set as 0.0, 0.25, 0.5 and 0.75 in different simulations to investigate its effect on soil behavior.

Table 1. Values of parameters for DEM simulation

Parameter	Value
Density ρ (kg/m^3)	2600
Normal stiffness of particle k_n^p (N/m)	1.5×10^{8}
Shear stiffness of particle k_s^p (N/m)	1.0×10^{8}
Normal stiffness of wall k_n^w (N/m)	1.5×10^{8}

Shear stiffness of wall k_s^w (N/m)	1.0 × 10^8
Friction coefficient of particle μ^p (–)	0.5
Initial friction coefficient of particle μ_{ini}^p (–)	0.0/0.1/1.0
Friction coefficient between wall and particle μ^w (–)	0.0
Rolling friction coefficient μ_r (–)	0.0/0.25/0.50/0.75

Figure 2 presents the evolution of shear stress and volumetric strain along with axial strain from samples with various particle shape conditions, in which the shear stress, τ, is given as

$$\tau = \frac{\sigma_1 - \sigma_3}{2} \qquad (4)$$

where σ_1 and σ_3 are the axial and confinement stress. For all the dense samples with various particle shape conditions, the shear stresses increase much faster compared with the corresponding loose samples until peak values are reached. Then the shear stresses decrease with the increase of axial strains. In addition, despite the difference in the initial relative density (80% versus 20%), the residual shear strengths of the dense and loose sample with same particle shape are almost identical, which conforms to the theory of critical soil mechanics. Both dense and loose samples contract at the beginning of the simulations and then change to dilative. However, the dense samples become dilative much earlier and have much larger volumetric strains than the corresponding loose ones. In Figure 2(a) and (b), the general evolution trends of shear stress and volumetric strain are quite similar for the T100 and S100 samples at both dense and loose conditions. However, the peak and residual strengths of the T100 sample are 77% and 49% higher than those of the S100 sample, which demonstrates the strong effect of particle shape on the shear strength of soils. This observation is consistent with experimental results reported by Cho et al.(2006) that soils made of particles with high angularity have a much large strength than soils made of round particles. The dilation of the T100 sample is more remarkable than that of the S100 sample at the dense state, while at the loose state the dilative behaviors of S100 and T100 samples are quite similar. When a soil sample consists of both SP and TP, the peak and residual shear strengths increase with an increase of the fraction of TP, as shown in In Figure 2(c). The evolutions of shear stress versus axial strain of the S75T25, S50T50 and S25T75 samples are bounded by a lower bound from the S100 sample and an upper bound from the T100 sample in Figure 2(a). The results of S100 samples with $\mu_r \neq 0$ are shown in Figure 2(e) and (f). In general, similar and reasonable trends of shear stress and volumetric strain versus axial strain are observed compared with SP or TP samples. As the rolling resistance coefficient of the S100 sample is increased from 0.25 to 0.75, the peak shear strength shows a remarkable increase from 254.1 kPa to 409.2 kPa. These observations indicate that the macroscopic shear properties of angular particles can be reasonable reproduced by adopting the rolling resistance method. Based on the critical state soil mechanics, the peak/residual friction angles of S100, T100, S75T25, S50T50, S25T75, S100 ($\mu_r = 0.25$), S100 ($\mu_r = 0.50$) and S100 ($\mu_r = 0.75$) are 24º/17º, 32º/24º, 26º/18º, 28º/21º, 30º/22º, 33º/24º, 39º/27º and 41º/29º respectively.

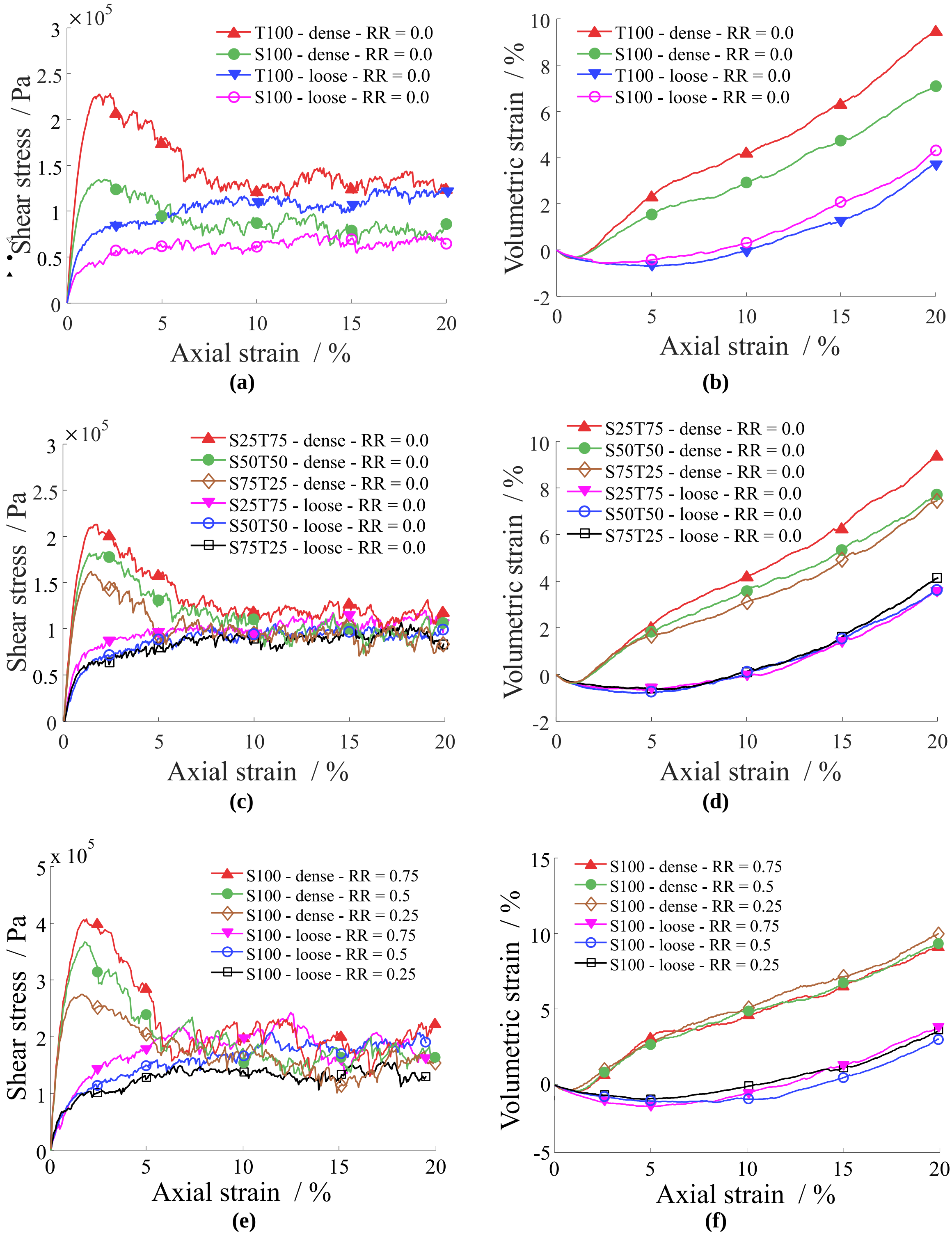

Figure 2. Shear stress and volumetric strain versus axial strain from simulations of biaxial tests on samples with: pure spherical and tetrahedral particles ((a) and (b)); a mixture of spherical and tetrahedral particles ((c) and (d)); and spherical particles with different rolling resistance coefficients ((e) and (f)) (RR: Rolling Resistance coefficient)

2.3. DEM modeling of caisson foundation insertion and failure

In a previous study conducted by the authors, the behaviors of a caisson foundation during the insertion, operation and failure processes were investigated micro-mechanically using 2D DEM (Wang and Yin, 2020). The schematic diagram of the caisson foundation model is shown in Figure 3. The sand had the same PSD with this study and soil particles were spherical without rolling resistance. The soil was prepared with the Multi-layer with Undercompaction Method (UCM) (Jiang and Yin, 2012, 2014; Jiang et al., 2003; Jiang et al., 2016) in order to obtain a homogeneous specimen. The caisson with both outer diameter and skirt length of 300 mm was assumed rigid and modeled with a particle clump. The caisson foundation the caisson was firstly slowly pushed into the soil at a constant velocity of 0.3 m/s until the caisson reached the final position. It worthwhile to mention that the loading rate is carefully chosen based on a sensitivity analysis to maintain the whole model at a quasi-static state. Then progressive failure of the caisson foundation at different loading combinations were investigated with the DEM model. Compared with the experimental results with same load combinations (Foglia et al., 2015), good agreements were found in various load-displacement curves which demonstrated the ability of this model to capture the behaviors of caisson foundation. Although the 2D caisson foundation model was used rather than the 3D to avoid high computation cost, the general trend of load-displacement curves and failure mechanisms were well captured and consistent with both experimental and theoretical results. A detailed description of the caisson foundation model can be found in (Wang and Yin, 2020) and will not be repeated here. In this study, the validated caisson foundation model is adopted to investigate effect of particle shape, which will be presented in the following section. Three different soil conditions, i.e. S100, T100 and S100 ($\mu_r = 0.5$), are used in the analysis. It takes about 26 hours on a workstation (Inter Xeon E5-2690A CPU and 128 GB RAM) to simulate one test from insertion process to the rotation angle of 5°.

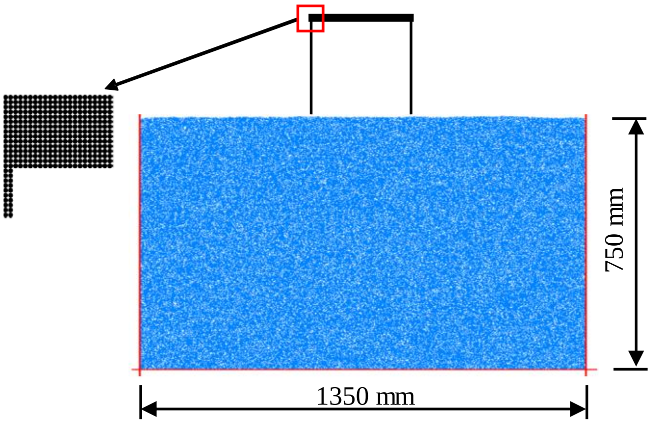

Figure 3. Schematic diagram of the caisson foundation model in DEM

3. Effect of particle shape on behavior of caisson foundation

In this section, caisson foundations with soils consisting of solely SP ($\mu_r = 0$), TP ($\mu_r = 0$) as well as SP ($\mu_r = 0.5$) are investigated. The model is subjected to a gravity of 10g to simulate a prototype caisson foundation with a diameter of 3 m. The ratio of dimensionally homogenous moment to horizontal load, M/(DH), is kept constant during the simulation. Three simulations with the M/(DH) of 1.1, 3.01 and 8.748, which are determined based on typically load conditions of wind turbines, are conducted. The moment and horizontal load increase monotonically until the rotational angle reaches 2°. Displacements and forces are monitored throughout the simulation.

3.1. Effect of particle shape on macroscopic behavior

Figure 4 presents the relationship between horizontal displacement (u) and horizontal load (H) for caisson foundations with different particle shapes. And the horizontal and rotational bearing capacities of different particles shapes are also summarized in Table 2. Results from simulations with different M/(DH)s and particle shapes exhibit a similar evolution trend: horizontal loads increase with the increase of horizontal displacements and then become stable. For a given M/(DH), simulations with SP ($\mu_r = 0.5$) has the largest horizontal loading capacity, which is around 80 % and 150 % higher than that from simulations with TP ($\mu_r = 0$) and SP ($\mu_r = 0$). In Figure 5, the rotational displacements (Dθ) increase as the dimensionally homogeneous moments (M/D) increase with a decreasing slope. Similar with the results of horizontal bearing capacity, the moment bearing capacity of simulations with SP ($\mu_r = 0.5$) is 65% and 110% higher than that of TP ($\mu_r = 0$) and SP ($\mu_r = 0$), respectively. The trends in Figure 5 and Figure 6 are similar to those observed in the experimental tests (Foglia et al., 2015), and indicate that both horizontal and moment bearing capacities of caisson foundation can be significantly increased by increasing the angularity of soil.

Table 2. Horizontal and rotational bearing capacities of different particles shapes (M/(DH)=1.1)

Particle shape	Horizontal bearing capacity (kN)	Rotational bearing capacity (kN·m)
SP ($\mu_r = 0$)	5.38	1.86
TP ($\mu_r = 0$)	7.32	2.40
SP ($\mu_r = 0.5$)	13.20	3.99

In Figure 6 and Figure 7, the evolution trends of both horizontal displacement (u) versus vertical displacement (w) and rotational displacement (Dθ) versus vertical displacement (w) can be reasonably characterized by a quasi-linear relationship, which have good agreement with the results reported in (Foglia et al., 2015). The influence of particle shape on the displacements is slight. Models with SP ($\mu_r = 0$) and TP ($\mu_r = 0$) share similar magnitudes of displacements (u, w and Dθ), while the displacements of model with SP ($\mu_r = 0.5$) are slightly larger. The increased magnitudes of displacement may be attributed to the larger dilation of angular particles as shown in Figure 2(c) and also reported in (Xiao et al., 2019).

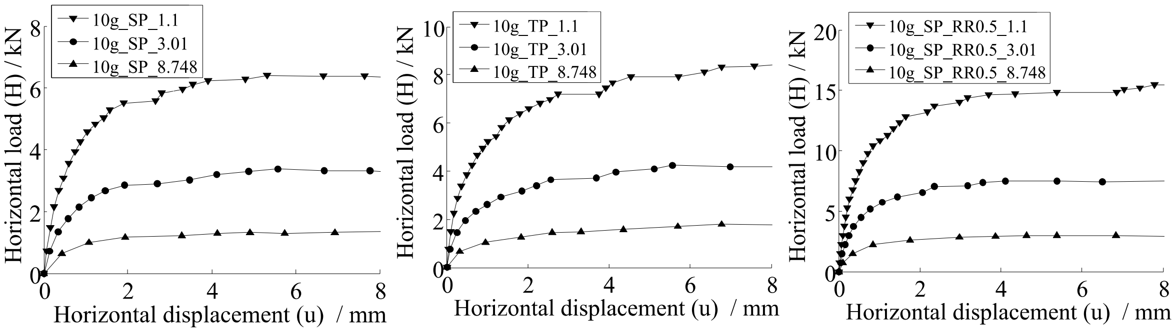

(a) (b) (c)

Figure 4. Horizontal displacement (u) versus horizontal load (H) from simulations with (a) SP ($\mu_r = 0$), (b) TP ($\mu_r = 0$) and (c) SP ($\mu_r = 0.5$)

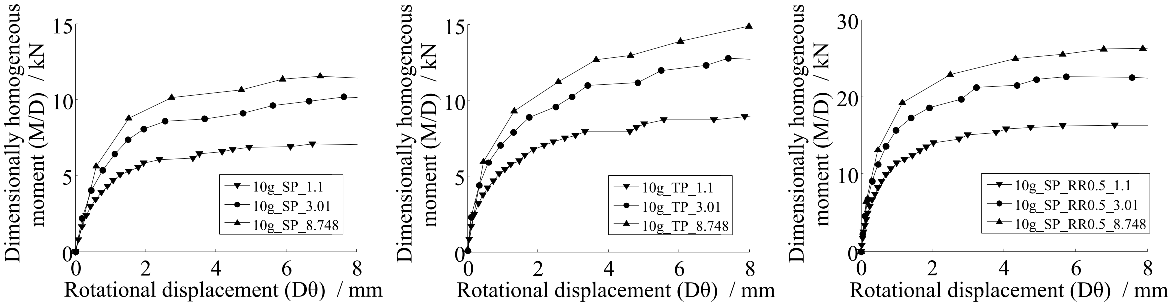

(a) (b) (c)

Figure 5. Rotational displacement (Dθ) versus dimensionally homogeneous moment (M/D) from simulations with (a) SP ($\mu_r = 0$), (b) TP ($\mu_r = 0$) and (c) SP ($\mu_r = 0.5$)

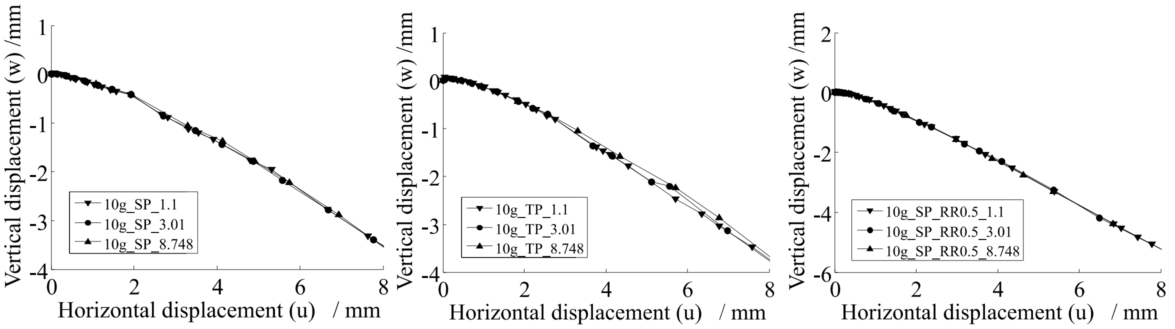

(a) (b) (c)

Figure 6. Horizontal displacement (u) versus vertical displacement (w) from simulations with (a) SP ($\mu_r = 0$), (b) TP ($\mu_r = 0$) and (c) SP ($\mu_r = 0.5$)

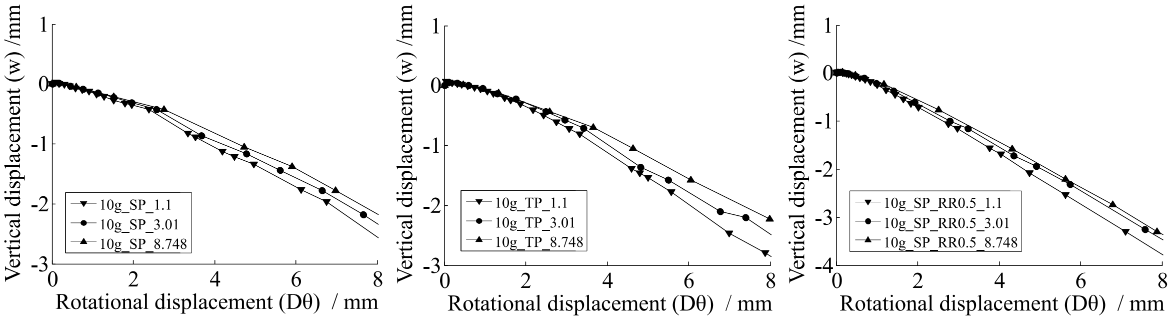

(a) (b) (c)

Figure 7. Rotational displacement (Dθ) versus vertical displacement (w) from simulations with (a) SP ($\mu_r = 0$), (b) TP ($\mu_r = 0$) and (c) SP ($\mu_r = 0.5$)

3.2. Effect of particle shape on microscopic behavior

The microscopic behavior of caisson foundation is discussed in this subsection in terms of particle rotation, particle displacement, APR (averaged micro-pure rotation rate) field, stress distribution and soil fabric. Note that only results from simulations with M/(DH) equal to 1.1 are presented, since models with different M/(DH)s share similar microscopic behavior. The foundation failure starts when the value of overturning moment becomes stable, which, according to Figure 5, corresponds a rotation angle of 1°. Therefore, the following analysis is based on the results with a rotation angle of 1°.

3.2.1. Micro-mechanical analysis

Figure 8 presents the particle rotation from simulations with different particle shapes. Because the caisson rotates counter clockwise, large particle rotation mainly occurs in the passive region on the left, in the active region on the right and inside the caisson. The particle rotation is negligible in the rest areas. The particles in the simulation with SP ($\mu_r = 0$) exhibit much larger particle rotation than TP ($\mu_r = 0$) and SP ($\mu_r = 0.5$), which is expected and can be attributed to less interlocking between smooth spherical particles. Because SP ($\mu_r = 0.5$) simulates a soil particle more angular than TP ($\mu_r = 0$) according to the results of biaxial tests in Figure 2, the magnitude of particle rotation in the simulation with SP ($\mu_r = 0.5$) is much smaller than that in the simulation with TP ($\mu_r = 0$).

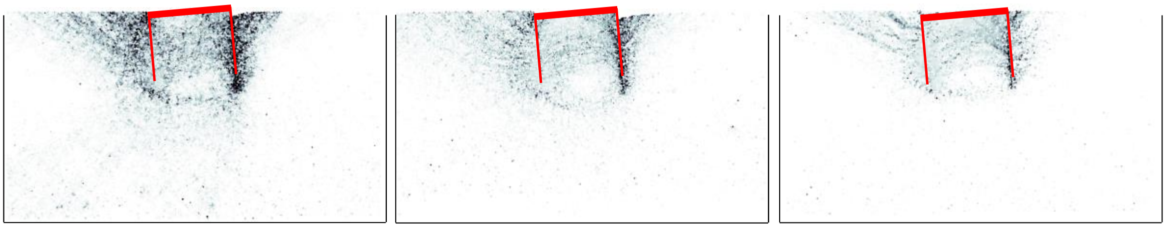

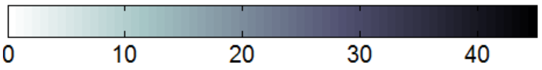

(a) (b) (c)

Figure 8. Particle rotation from simulations with (a) SP ($\mu_r = 0$), (b) TP ($\mu_r = 0$) and (c) SP ($\mu_r = 0.5$)

Figure 9 shows the particle displacement field from simulations with different particle shapes. The shapes of the displacement fields in Figure 9(a), (b) and (c) are similar. The passive failure region and active failure region can be clearly identified on the left and right of the caisson in each simulation. The maximum soil displacement happens at the ground surface. Identifying the rotation center is important to understand the failure mechanism of caisson foundation, and many studies have been conducted to find its location (Tang et al., 2016). In Figure 9, the rotation center of caisson foundation is located at the lower left part of the caisson, which has a buried depth of 0.67, 0.68 and 0.75 times of skirt length respectively for simulations with SP ($\mu_r = 0$), TP ($\mu_r = 0$) and SP ($\mu_r = 0.5$). The values found in this study is within the range of theoretical estimation that the rotation center has a depth from infinite to two-third of skirt length depending on the embedded length of caisson foundation (Tang et al., 2016).

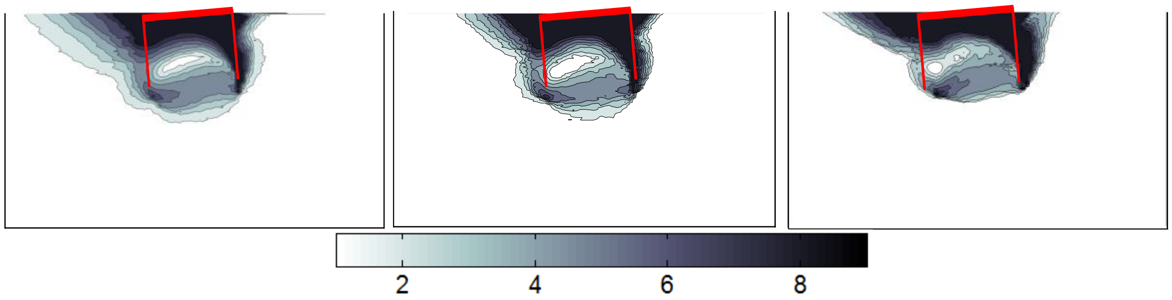

(a) (b) (c)

Figure 9. Particle displacement field from simulations with (a) SP ($\mu_r = 0$), (b) TP ($\mu_r = 0$) and (c) SP ($\mu_r = 0.5$)

The movement of caisson also significantly changes the vertical and horizontal distributions in ground, as shown in Figure 10 to. Because of the counter clockwise movement of the caisson, the soils outside the left skirt (passive zone) become more compacted which causes both vertical and horizontal stresses increase. While in the active zone on the right, stresses are decreased. In addition, stress increase is also observed in the lower left part of the soil plug, which is due to the rotation of the caisson around the rotation center in Figure 9. The particle shape has a strong influence on the stress distribution. The introduction of rolling resistance increases the interlocking between particle by significantly decreasing the relative rotational movement within contacts (Yang et al., 2017). Therefore, stress increase is more evident in simulation with SP ($\mu_r = 0.5$). Similarly, simulation with TP ($\mu_r = 0$) experiences stronger stress increase than that of the simulation with SP ($\mu_r = 0$).

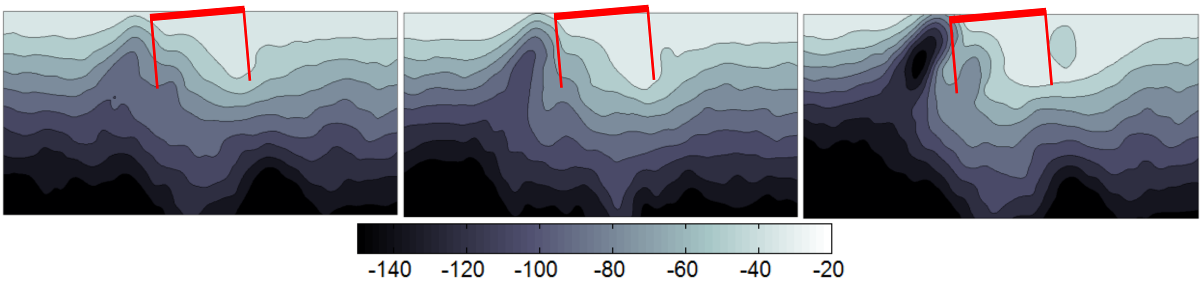

(a) **(b)** **(c)**

Figure 10. Vertical stress distribution (kPa) in ground from simulations with (a) SP ($\mu_r = 0$), (b) TP ($\mu_r = 0$) and (c) SP ($\mu_r = 0.5$)

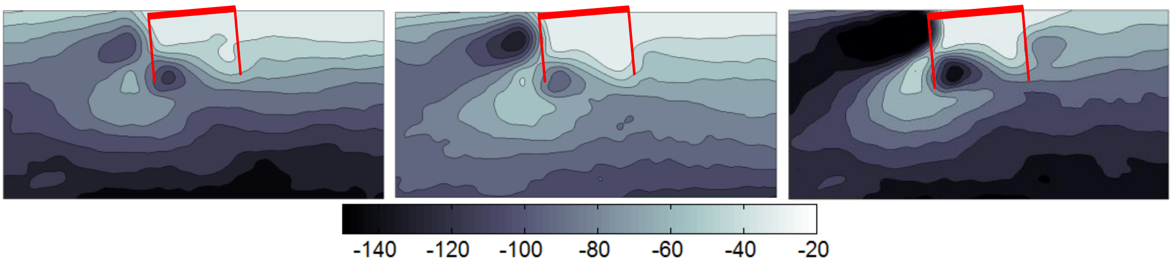

(a) **(b)** **(c)**

Figure 11. Horizontal stress distribution (kPa) in ground from simulations with (a) SP ($\mu_r = 0$), (b) TP ($\mu_r = 0$) and (c) SP ($\mu_r = 0.5$)

The force chain distributions from simulations with different particle shape are shown in Figure 12, which show the localized large force concentration induced by caisson movements. The density and magnitude of force chains near the upper left and the lower right of the caisson, as well as in the lower left part of the soil plug are much higher than other areas. Because the stress distributions are the average of contact force within measure spheres in DEM, the locations of large contact force match very well with the stress distributions in Figure 10 and Figure 11. The particle shape does not affect the contact force concentration but has a strong influence on the magnitude of the contact force. The maximum contact force increases with the particle angularity and rolling resistance coefficient because of the increased interlocking force among particles.

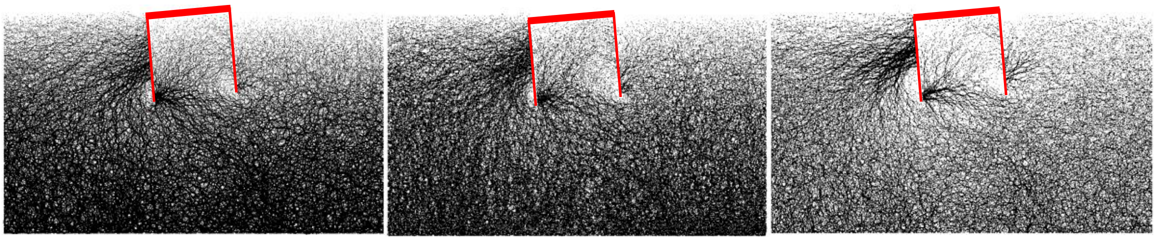
(a) (b) (c)

Figure 12. Force chain distribution when particle shape and maximum contact force are SP ($\mu_r = 0$) and 2.2 kN (a), TP ($\mu_r = 0$) and 2.7 kN (b) and SP ($\mu_r = 0.5$) and 5.7 kN (c)

3.2.2. Fabric analysis

According to numerous previous studies, soil behaviors at macroscale are closely related to the fabric of particles, i.e. internal micro-structure and arrangement. Qualitative and quantitative results have been reported about the relationship between particle fabric and macroscale properties of soils such as dilation, strain localization, permeability and liquefaction (!!! INVALID CITATION !!! (Gao and Zhao, 2013; Little et al., 1992; Wang et al., 2019b; Yimsiri and Soga, 2010)). Contact-based fabric descriptors, such as contact normal distribution and contact force distribution, are widely used in static or quasi-static analysis under various loading conditions (Gu et al., 2014; Guo and Zhao, 2013). In addition, void-based descriptors are also proposed and is more preferable to liquefied soils in which almost all contacts are lost (Wang and Wei, 2016; Wei et al., 2018). Particle shape has a significant effect on soil fabric. For example, there are obvious differences in the contact force distribution in soils with different particle shapes (Antony and Kuhn, 2004), and the branch vector (contact normal) has direct relationship with particle shape (Ng, 2009). Therefore, in order to better understand the effect of particle shape, the fabric evolution is analyzed.

Based on the analysis in Section 3.2.1, particle behaviors are significantly different in different regions, which indicates strong variations of particle fabric. Therefore, for the sake of better understanding the effect of particle shape, the soil particles are divided into four groups depending on their positions. Schematic diagram of grouping method is shown in Figure 13. The triangular region on the left of the caisson, which has the LS particle group, represents the passive failure zone. While the triangle on the right is the active zone and has the RS group. Particles inside the caisson belongs to the IN group, and the rest particles are in the OUT group. The angle between the active region and horizon is assumed to be 30° which is obtained by $45^{\circ}-\phi_{p\_ave}/2$, where the ϕ_{p_ave} (30°) is the average peak friction angle of the soils with SP ($\mu_r=0$), TP ($\mu_r=0$) and SP ($\mu_r=0.5$). Similarly, $45^{\circ}+\phi_{p\_ave}/2$ is used for the active region.

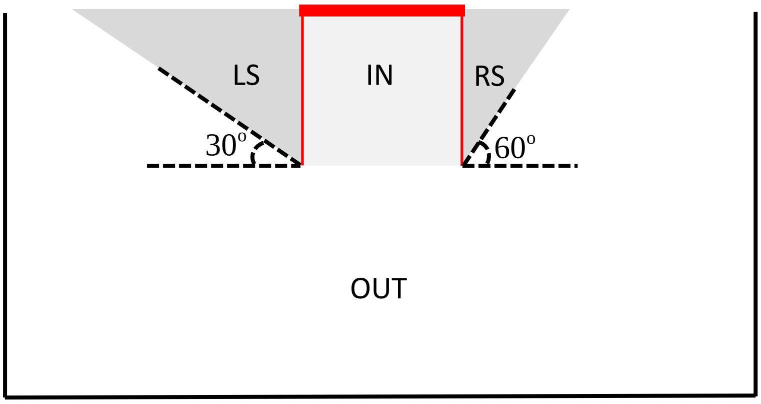

Figure 13. Schematic diagram of soil particle groups

Three commonly used contact-based fabric descriptors, i.e. particle contact orientation, normal and shear contact force, are examined. Their angular distributions are given as (Rothenburg and Bathurst, 1989)

$$E(\theta)=\frac{1}{2\pi}[1+a\cos 2(\theta-\theta_a)] \qquad (5)$$

$$f_n(\theta) = f_{n0}[1 + a_n \cos 2(\theta - \theta_n)] \quad (6)$$

and

$$f_s(\theta) = -f_{s0} a_s \sin 2(\theta - \theta_s) \quad (7)$$

where $E(\theta) / f_n(\theta) / f_s(\theta)$ is the angular distribution of particle contact orientation/normal contact force/shear contact force; f_{n0} / f_{s0} is the average normal/shear contact force; $a / a_n / a_s$ is the magnitude of anisotropy for the three descriptors; and $\theta_a / \theta_n / \theta_s$ is the principal direction of anisotropy. Detailed derivation of Eq. (5) to Eq. (7) can be found in (Rothenburg and Bathurst, 1989).

Before the rotational movement, the distributions of contact normal and normal contact force have an oval shape which is induced by the horizontal compaction during the insertion of the caisson (Wang and Yin, 2020). Similarly, the shear contact force is also mainly distributed in the horizontal direction. After the rotational movement of the caisson, the fabric is significantly changed. Figure 14 and Figure 15 show the contact orientation and contact force distributions of different particle shapes respectively in the LS and RS group, in which the black lines are data obtained from DEM simulations and the red lines represents the analytical approximations based on Eq. (5) to Eq. (7). For particles in both groups, strong anisotropy can be observed for soils with different particle shapes and the analytical approximations match well with the numerical results. The principal directions of anisotropy are mainly determined by the rotational direction of the caisson and only slightly affected by the particle shape. For example, in Figure 14 the principal directions of contact orientation for particles in LS are within 5º difference (14º, 14º and 19º for different particle shapes), and the difference of the principal directions of normal and shear contact force are 2º and 7º. In Figure 15 the difference in principal directions for particles in the RS group are 22º, 13º and 16º respectively for contact orientation, normal and shear contact force, which are much larger than those for particles in LS group. This observation is due to the fact that in the passive region the overwhelming passive force becomes a dominating influencing factor for the principal direction of anisotropy and undermines the other ones such as particle shape. Similar observation is also found in (Yin et al., 2020).

The particle shape plays an important role in the magnitude of the anisotropy. For particles in the LS group in Figure 14, the magnitude of contact orientation anisotropy for SP ($\mu_r = 0.5$) is 41% and 11% higher that of SP ($\mu_r = 0$) and TP ($\mu_r = 0$). In terms of magnitude of anisotropy of normal contact force, SP ($\mu_r = 0.5$) is also 67% and 38% higher. In Figure 14(c), (f) and (i), magnitudes of anisotropy of shear contact force for are similar for different particle shapes which indicates that the movement of caisson does not generate large shear force at the particle scale. In other words, force is transmitted mainly in the normal direction than the shear direction. In the active region, the magnitude of anisotropy for angular particles are even higher than SP as shown in Figure 15: SP ($\mu_r = 0.5$) is 70% and 7% higher in contact orientation, and 111% and 64% higher in contact normal force than those of SP ($\mu_r = 0$) and TP ($\mu_r = 0$).

Anisotropy is also generated in particle groups such as IN and OUT, which is summarized in Table 3. The magnitude of anisotropy of contact orientation and normal contact force (a and a_n) for soils in the LS and RS groups are much larger than particles in other groups, which demonstrates the large anisotropy in the active and passive region. These results are consistent with the observations in Figure 8 to Figure 12. To sum up, the movement of caisson introduces strong anisotropy in the passive and active regions, and the particle shape has a significant influence on the magnitude of the anisotropy.

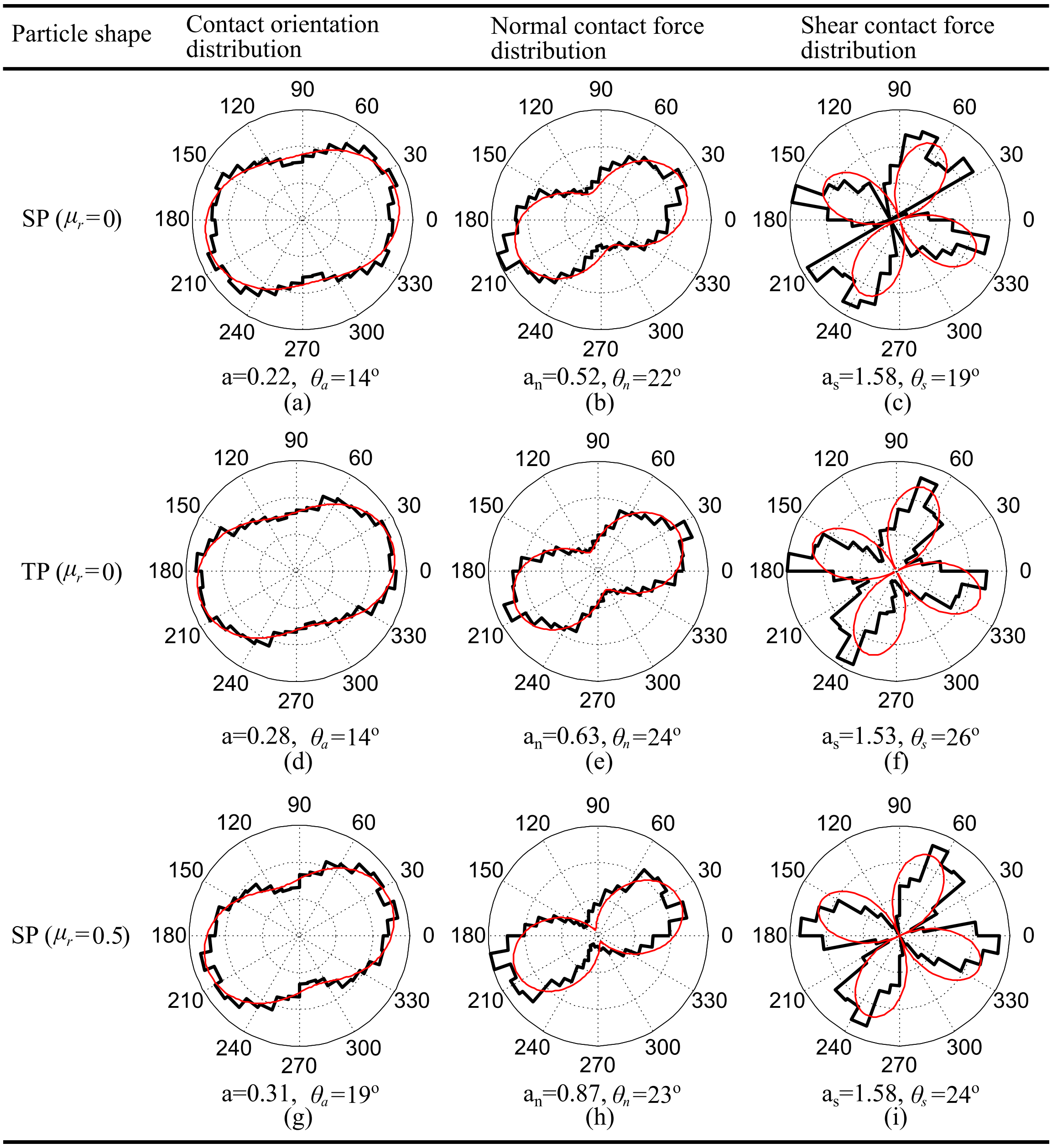

Figure 14. Contact orientation and contact force distributions of particles in the LS group

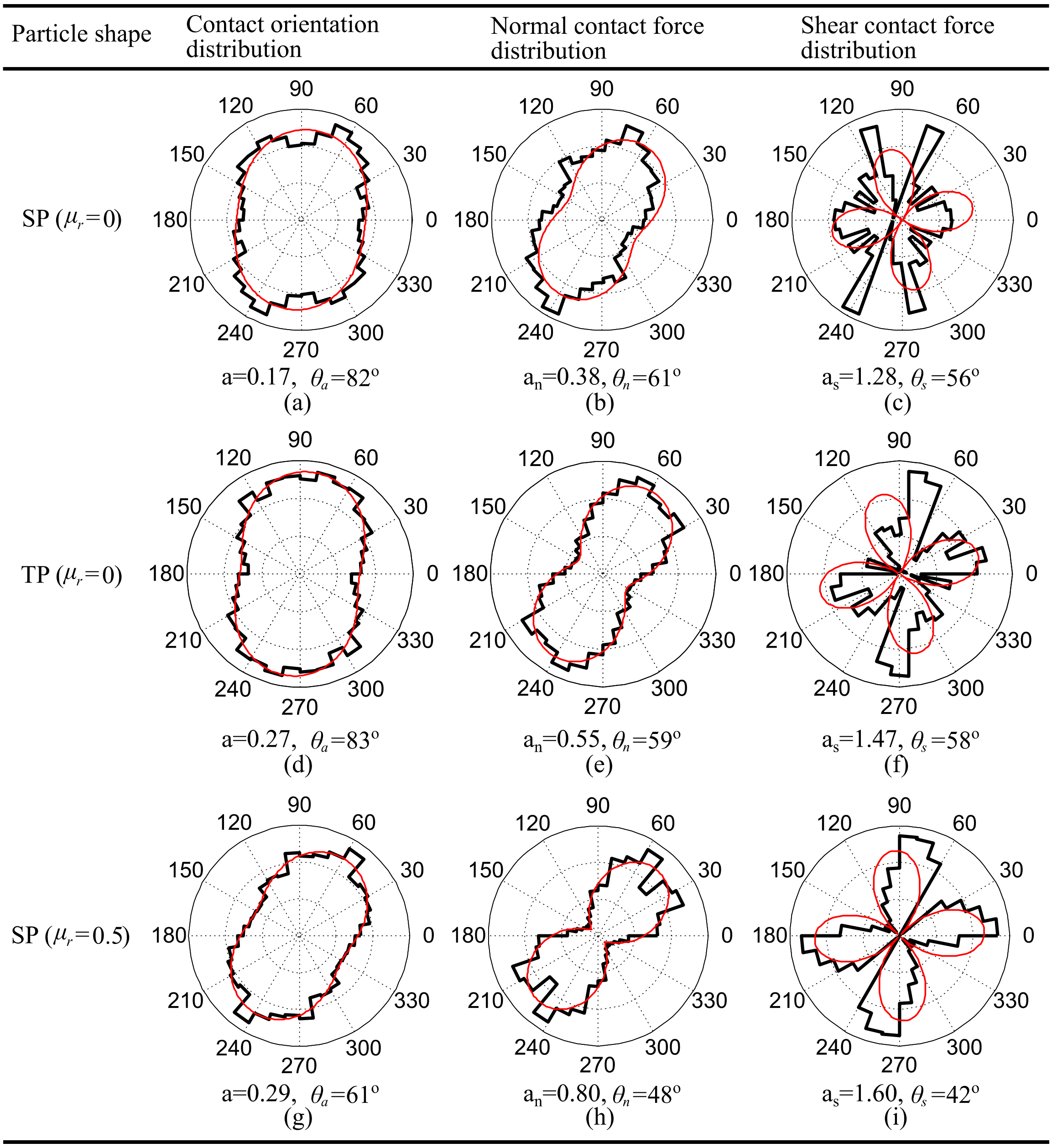

Figure 15. Contact orientation and contact force distributions of particles in the RS group

Table 3. Summary of soil anisotropy induced by the foundation failure

Fabric descriptor		SP ($\mu_r=0$)				TP ($\mu_r=0$)				SP ($\mu_r=0.5$)			
		LS	RS	IN	OUT	LS	RS	IN	OUT	LS	RS	IN	OUT
Contact orientation	a (-)	0.22	0.17	0.10	0.02	0.28	0.27	0.16	0.07	0.31	0.29	0.16	0.02
	θ_a (°)	14	82	43	10	14	83	49	88	19	61	17	5
Normal contact force	a_n (-)	0.52	0.38	0.24	0.01	0.63	0.55	0.35	0.15	0.87	0.80	0.41	0.06
	θ_n (°)	22	61	37	-9	24	59	47	90	23	48	27	12
Shear contact force	a_s (-)	1.58	1.28	1.54	1.27	1.53	1.47	1.55	1.58	1.58	1.60	1.51	1.46
	θ_s (°)	19	56	34	-4	26	58	50	89	24	42	22	17

4. Conclusions

In this paper, the caisson foundation has been analyzed with DEM, in which the effect of particle shape has been discussed by using spherical particle, tetrahedral particle as well as spherical particle with rolling resistance. In order to obtain the soil properties, a series of biaxial tests have been modeled on samples with different particle shape, and typical shear behaviors have been observed in all simulations. The caisson foundation model based on DEM, which was validated in a previous study by the authors, has been used in this investigation. The effect of particle shape on the macro- and microscopic behaviors of caisson foundation has then been investigated with different loading conditions. Conclusions are made as follows:

(1) At the macroscale, caisson foundation with angular particles or spherical particles with rolling resistance has an increased horizontal and rotational bearing capacities, which can be explained by the fact that soil critical friction angle increases with the soil angularity. In addition, caisson foundation with spherical particles ($\mu_r = 0.5$) exhibits slightly larger magnitudes of both rotational and translational displacements due to the increased soil dilation.

(2) At the microscale, the movement of caisson generates much smaller particle rotation in soils made of angular particles and spherical particles with rolling resistance due to the strong interlocking capacity between particles. In addition, the stress concentration and magnitude of force chains for angular particles and spherical particles with rolling resistance are much larger than those of spherical particles.

(3) In terms of soil fabric, the movement of caisson introduces strong anisotropy in both passive and active regions, and the particle shape has a significant influence on the magnitude of the anisotropy.

Because particle shape has a strong influence on soil properties, it is important to account for the effect of particle shape in the analysis of caisson foundation. This study has been carried out to improve the understanding of the effect of particle shape at both macro- and microscale and provide helpful guidance on the design of caisson foundation. It is also worth noting that in order to focus on the effect of particle shape, some assumptions and simplifications are made which may impose some limitations for this study. For example, particles are uncrushable in all simulations. In real engineering practices of caisson foundation, the penetration force at the caisson tip and the rotational movement are likely to induce some particle breakage, which has a strong influence on the behavior of granular soils (Coop et al., 2004; de Bono and Mcdowell, 2016; Zhou et al., 2020). However, particle breakage is a complex problem which is beyond the scope of this study, and therefore is not considered. In addition, soil used in this study is dry sand which is same with the experiments (Foglia et al., 2015), so that the results from DEM simulations and experiments are comparable. In addition, the peak friction angle obtained from the biaxial tests are higher compared with experimental results (Wu et al., 2017). This limitation can be explained that 2D particles are restricted in a plane which tends to exhibit a larger dilation and therefore higher peak strength (Jing et al., 2018).

Acknowledgement

This research was financially supported by the Key Special Project for Introduced Talents Team of Southern Marine Science and Engineering Guangdong Laboratory (Guangzhou) (No.: GML2019ZD0503). The authors also would like to thank Mr. Honghao Lu who conducted a lot of numerical simulations for this study.

References

Zhu et al., 2019!!! INVALID CITATION !!! (Bagheri et al., 2017; Kelly et al., 2006; Yun and Bransby, 2007).

!!! INVALID CITATION !!! (Gao and Zhao, 2013; Little et al., 1992; Wang et al., 2019b; Yimsiri and Soga, 2010).

Achmus, M., Akdag, C.T., and Thieken, K., 2013. Load-bearing behavior of suction bucket foundations in sand. Applied Ocean Research, **43**: 157-165.

Afzali-Nejad, A., Lashkari, A., and Shourijeh, P.T., 2017. Influence of particle shape on the shear strength and dilation of sand-woven geotextile interfaces. Geotextiles and Geomembranes, **45**(1): 54-66.

Ai, J., Chen, J.F., Rotter, J.M., and Ooi, J.Y., 2011. Assessment of rolling resistance models in discrete element simulations. Powder Technology, **206**(3): 269-282.

Alonso-Marroquin, F., Muhlhaus, H.B., and Herrmann, H.J., 2008. Micromechanical investigation of granular ratcheting using a discrete model of polygonal particles. Particuology, **6**(6): 390-403.

Antony, S.J., and Kuhn, M.R., 2004. Influence of particle shape on granular contact signatures and shear strength: new insights from simulations. International Journal of Solids and Structures, **41**(21): 5863-5870.

Bagheri, P., Son, S.W., and Kim, J.M., 2017. Investigation of the load-bearing capacity of suction caissons used for offshore wind turbines. Applied Ocean Research, **67**: 148-161.

Barari, A., and Ibsen, L.B., 2012. Undrained response of bucket foundations to moment loading. Applied Ocean Research, **36**: 12-21.

Byrne, B.W., and Houlsby, G.T., 2002. Experimental investigations of response of suction caissons to transient vertical loading. Journal of Geotechnical and Geoenvironmental Engineering, **128**(11): 926-939.

Cassidy, M.J., Randolph, M.F., and Byrne, B.W., 2006. A plasticity model describing caisson behaviour in clay. Applied Ocean Research, **28**(5): 345-358.

Cavarretta, I., Coop, M., and O'Sullivan, C., 2010. The influence of particle characteristics on the behaviour of coarse grained soils. Geotechnique, **60**(6): 413-423.

Chang, K.C., Sung, Y.C., Liu, K.Y., Wang, P.H., Lee, Z.K., Lee, L.S., and Witarto. 2014. Seismic performance of an existing bridge with scoured caisson foundation. Earthquake Engineering and Engineering Vibration, **13**: 151-165.

Chen, Y.D., Deng, A., Wang, A.T., and Sun, H.S., 2018. Performance of screw-shaft pile in sand: Model test and DEM simulation. Computers and Geotechnics, **104**: 118-130.

Cho, G.C., Dodds, J., and Santamarina, J.C., 2006. Particle shape effects on packing density, stiffness, and strength: Natural and crushed sands. Journal of Geotechnical and Geoenvironmental Engineering, **132**(5): 591-602.

Coop, M.R., Sorensen, K.K., Freitas, T.B., and Georgoutsos, G., 2004. Particle breakage during shearing of a carbonate sand. Geotechnique, **54**(3): 157-163.

Cox, J.A., O'Loughlin, C.D., Cassidy, M., Bhattacharya, S., Gaudin, C., and Bienen, B., 2014. Centrifuge study on the cyclic performance of caissons in sand. International Journal of Physical Modelling in Geotechnics, **14**(4): 99-115.

Cui, S., Tan, Y., and Lu, Y., 2020. Algorithm for generation of 3D polyhedrons for simulation of rock particles by DEM and its application to tunneling in boulder-soil matrix. Tunnelling and Underground Space Technology, **106**: 103588.

de Bono, J., and Mcdowell, G., 2016. Particle breakage criteria in discrete-element modelling. Geotechnique, **66**(12): 1014-1027.

Fan, H., Huang, D.R., Wang, G., and Wang, J.F., 2020. Discontinuous deformation analysis for SH-body. Computers and Geotechnics, **117**.

Foglia, A., Gottardi, G., Govoni, L., and Ibsen, L.B., 2015. Modelling the drained response of bucket foundations for offshore wind turbines under general monotonic and cyclic loading. Applied Ocean Research, **52**: 80-91.

Fu, R., Hu, X.L., and Zhou, B., 2017. Discrete element modeling of crushable sands considering realistic particle shape effect. Computers and Geotechnics, **91**: 179-191.

Gong, J., Nie, Z.H., Zhu, Y.G., Liang, Z.Y., and Wang, X., 2019. Exploring the effects of particle shape and content of fines on the shear behavior of sand-fines mixtures via the DEM. Computers and Geotechnics, **106**: 161-176.

Gu, X.Q., Huang, M.S., and Qian, J.G., 2014. DEM investigation on the evolution of microstructure in granular soils under shearing. Granular Matter, **16**(1): 91-106.

Guises, R., Xiang, J.S., Latham, J.P., and Munjiza, A., 2009. Granular packing: numerical simulation and the characterisation of the effect of particle shape. Granular Matter, **11**(5): 281-292.

Guo, N., and Zhao, J.D., 2013. The signature of shear-induced anisotropy in granular media. Computers and Geotechnics, **47**: 1-15.

Huang, Q.S., Zhou, W., Ma, G., Ng, T.T., and Xu, K., 2020. Experimental and numerical investigation of Weibullian behavior of grain crushing strength. Geoscience Frontiers, **11**(2): 401-411.

Jia, N., Zhang, P.Y., Liu, Y.G., and Ding, H.Y., 2018. Bearing capacity of composite bucket foundations for offshore wind turbines in silty sand. Ocean Engineering, **151**: 1-11.

Jiang, M.J., and Yin, Z.Y., 2012. Analysis of stress redistribution in soil and earth pressure on tunnel lining using the discrete element method. Tunnelling and Underground Space Technology, **32**: 251-259.

Jiang, M.J., and Yin, Z.Y., 2014. Influence of soil conditioning on ground deformation during longitudinal tunneling. Comptes Rendus Mecanique, **342**(3): 189-197.

Jiang, M.J., Konrad, J.M., and Leroueil, S., 2003. An efficient technique for generating homogeneous specimens for DEM studies. Computers and Geotechnics, **30**(7): 579-597.

Jiang, M.J., Yu, H.S., and Harris, D., 2005. A novel discrete model for granular material incorporating rolling resistance. Computers and Geotechnics, **32**(5): 340-357.

Jiang, M.J., Yin, Z.Y., and Shen, Z.F., 2016. Shear band formation in lunar regolith by discrete element analyses. Granular Matter, **18**(2): 32.

Jin, Z., Yin, Z.Y., Kotronis, P., and Jin, Y.F., 2019a. Numerical investigation on evolving failure of caisson foundation in sand using the combined Lagrangian-SPH method. Marine Georesources & Geotechnology, **37**(1): 23-35.

Jin, Z., Yin, Z.Y., Kotronis, P., and Li, Z., 2019b. Advanced numerical modelling of caisson foundations in sand to investigate the failure envelope in the H-M-V space. Ocean Engineering, **190**: 106394.

Jin, Z., Yin, Z.Y., Kotronis, P., Li, Z., and Tamagnini, C., 2019c. A hypoplastic macroelement model for a caisson foundation in sand under monotonic and cyclic loadings. Marine Structures, **66**: 16-26.

Jing, X.Y., Zhou, W.H., Zhu, H.X., Yin, Z.Y., and Li, Y.M., 2018. Analysis of soil-structural interface behavior using three-dimensional DEM simulations. International Journal for Numerical and Analytical Methods in Geomechanics, **42**(2): 339-357.

Kawamoto, R., Ando, E., Viggiani, G., and Andrade, J.E., 2016. Level set discrete element method for three-dimensional computations with triaxial case study. Journal of the Mechanics and Physics of Solids, **91**: 1-13.

Kelly, R.B., Houlsby, G.T., and Byrne, B.W., 2006. A comparison of field and laboratory tests of caisson foundations in sand and clay. Geotechnique, **56**(9): 617-626.

Kou, H.L., Yang, D.L., Zhang, W.C., Wu, Y.F., and Fu, Q., 2019. Model tests on performance of offshore wind turbine with suction caisson foundation in sand. Marine Georesources & Geotechnology.

Mehravar, M., Harireche, O., and Faramarzi, A., 2016. Evaluation of undrained failure envelopes of caisson foundations under combined loading. Applied Ocean Research, **59**: 129-137.

Mehravar, M., Harireche, O., Faramarzi, A., and Alani, A.M., 2017. Modelling the variation of suction pressure during caisson installation in sand using FLAC3D. Ships and Offshore Structures, **12**(7): 893-899.

Ng, T.T., 2009. Particle shape effect on macro- and micro-behaviors of monodisperse ellipsoids. International Journal for Numerical and Analytical Methods in Geomechanics, **33**(4): 511-527.

Nguyen-Sy, L., and Houlsby, G.T., 2005. The theoretical modelling of a suction caisson foundation using hyperplasticity theory. Frontiers in Offshore Geotechnics II, Perth: 417.

Peng, X.Y., Zhang, L.L., Jeng, D.S., Chen, L.H., Liao, C.C., and Yang, H.Q., 2017. Effects of cross-correlated multiple spatially random soil properties on wave-induced oscillatory seabed response. Applied Ocean Research, **62**: 57-69.

Podczeck, F., and Miah, Y., 1996. The influence of particle size and shape on the angle of internal friction and the flow factor of unlubricated and lubricated powders. International Journal of Pharmaceutics, **144**(2): 187-194.

Rothenburg, L., and Bathurst, R.J., 1989. Analytical Study of Induced Anisotropy in Idealized Granular-Materials. Geotechnique, **39**(4): 601-614.

Rousé, P.C., Fannin, R.J., and Shuttle, D.A., 2008. Influence of roundness on the void ratio and strength of uniform sand. Geotechnique, **58**(3): 227-231.

Salazar, A., Saez, E., and Pardo, G., 2015. Modeling the direct shear test of a coarse sand using the 3D Discrete Element Method with a rolling friction model. Computers and Geotechnics, **67**: 83-93.

Shinohara, K., Oida, M., and Golman, B., 2000. Effect of particle shape on angle of internal friction by triaxial compression test. Powder Technology, **107**(1-2): 131-136.

Skau, K.S., Grimstad, G., Page, A.M., Eiksund, G.R., and Jostad, H.P., 2018. A macro-element for integrated time domain analyses representing bucket foundations for offshore wind turbines. Marine Structures, **59**: 158-178.

Sui, T.T., Jin, Y., Wang, Z.J., Zhang, C., and Shi, J., 2019. Effects of the Soil Property Distribution Gradient on the Wave-Induced Response of a Non-Homogeneous Seabed. Journal of Marine Science and Engineering, **7**(8).

Tang, X.W., Zhang, X.W., Shao, Q., and Li, Z.Q., 2016. Rotation Center and Horizontal Bearing Capacity of the Bucket Foundation in Soft Ground. Marine Georesources & Geotechnology, **34**(6): 594-601.

Thusyanthan, I., 2012. Seabed Soil Classification, Soil Behaviour, and Pipeline Design. Offshore Technology Conference.

Ting, J.M., Khwaja, M., Meachum, L.R., and Rowell, J.D., 1993. An Ellipse-Based Discrete Element Model for Granular-Materials. International Journal for Numerical and Analytical Methods in Geomechanics, **17**(9): 603-623.

Villalobos, F.A., Byrne, B.W., and Houlsby, G.T., 2009. An Experimental Study of the Drained Capacity of Suction Caisson Foundations under Monotonic Loading for Offshore Applications. Soils and Foundations, **49**(3): 477-488.

Wang, G., and Wei, J.T., 2016. Microstructure evolution of granular soils in cyclic mobility and post-liquefaction process. Granular Matter, **18**(3).

Wang, P., and Arson, C., 2018. Energy distribution during the quasi-static confined comminution of granular materials. Acta Geotechnica, **13**(5): 1075-1083.

Wang, P., and Yin, Z.-Y., 2020. Micro-mechanical analysis of caisson foundation in sand using DEM. Ocean Engineering, **203**: 107240.

Wang, P., Karatza, Z., and Arson, C., 2019. DEM modelling of sequential fragmentation of zeolite granules under oedometric compression based on XCT observations. Powder Technology, **347**: 66-75.

Wang, P., Gao, N., Ji, K., Stewart, L., and Arson, C., 2020. DEM analysis on the role of aggregates on concrete strength. Computers and Geotechnics, **119**: 103290.

Wei, J.T., Huang, D.R., and Wang, G., 2018. Microscale Descriptors for Particle-Void Distribution and Jamming Transition in Pre- and Post-Liquefaction of Granular Soils. Journal of Engineering Mechanics, **144**(8).

Wensrich, C.M., and Katterfeld, A., 2012. Rolling friction as a technique for modelling particle shape in DEM. Powder Technology, **217**: 409-417.

Wood, D.M., and Maeda, K., 2008. Changing grading of soil: effect on critical states. Acta Geotechnica, **3**(1): 3-14.

Wu, K., Abriak, N., Becquart, F., Pizette, P., Remond, S., and Liu, S., 2017. Shear mechanical behavior of model materials samples by experimental triaxial tests: case study of 4 mm diameter glass beads. Granular Matter, **19**(4): 65.

Xiang, Y.Z., Liu, H.L., Zhang, W.G., Chu, J., Zhou, D., and Xiao, Y., 2018. Application of transparent soil model test and DEM simulation in study of tunnel failure mechanism. Tunnelling and Underground Space Technology, **74**: 178-184.

Xiao, Y., Long, L., Matthew Evans, T., Zhou, H., Liu, H., and Stuedlein Armin, W., 2019. Effect of Particle Shape on Stress-Dilatancy Responses of Medium-Dense Sands. Journal of Geotechnical and Geoenvironmental Engineering, **145**(2): 04018105.

Yang, J., and Wei, L.M., 2012. Collapse of loose sand with the addition of fines: the role of particle shape. Geotechnique, **62**(12): 1111-1125.

Yang, J., and Luo, X.D., 2015. Exploring the relationship between critical state and particle shape for granular materials. Journal of the Mechanics and Physics of Solids, **84**: 196-213.

Yang, Y., Cheng, Y.M., and Sun, Q.C., 2017. The effects of rolling resistance and non-convex particle on the mechanics of the undrained granular assembles in 2D. Powder Technology, **318**: 528-542.

Yin, Z.-Y., Wang, P., and Zhang, F., 2020. Effect of particle shape on the progressive failure of shield tunnel face in granular soils by coupled FDM-DEM method. Tunnelling and Underground Space Technology, **100**: 103394.

Yun, G., and Bransby, M.F., 2007. The undrained vertical bearing capacity of skirted foundations. Soils and Foundations, **47**(3): 493-505.

Zhang, D.M., Gao, C.P., and Yin, Z.Y., 2019. CFD-DEM modeling of seepage erosion around shield tunnels. Tunnelling and Underground Space Technology, **83**: 60-72.

Zhang, Q., Xu, W.Y., Liu, Q.Y., Wang, W., and Meng, Q.X., 2017. A novel non-overlapping approach to accurately represent 2D arbitrary particles for DEM modelling. Journal of Central South University, **24**(1): 190-202.

Zhao, B., An, X.Z., Wang, Y., Zhao, H.Y., Shen, L.L., Sun, X.D., and Zou, R.P., 2020. Packing of different shaped tetrahedral particles: DEM simulation and experimental study. Powder Technology, **360**: 21-32.

Zhou, W., Ma, G., Chang, X.L., and Zhou, C.B., 2013. Influence of Particle Shape on Behavior of Rockfill Using a Three-Dimensional Deformable DEM. Journal of Engineering Mechanics, **139**(12): 1868-1873.

Zhou, W., Huang, Y., Ng, T.T., and Ma, G., 2018a. A geometric potential-based contact detection algorithm for egg-shaped particles in discrete element modeling. Powder Technology, **327**: 152-162.

Zhou, W., Wu, W., Ma, G., Ng, T.T., and Chang, X.L., 2018b. Undrained behavior of binary granular mixtures with different fines contents. Powder Technology, **340**: 139-153.

Zhou, W., Wang, D., Ma, G., Cao, X.X., Hu, C., and Wu, W., 2020. Discrete element modeling of particle breakage considering different fragment replacement modes. Powder Technology, **360**: 312-323.

Zhou, W.H., Jing, X.Y., Yin, Z.Y., and Geng, X.Y., 2019. Effects of particle sphericity and initial fabric on the shearing behavior of soil-rough structural interface. Acta Geotechnica, **14**(6): 1699-1716.

Zhu, B., Kong, D.Q., Chen, R.P., Kong, L.G., and Chen, Y.M., 2011. Installation and lateral loading tests of suction caissons in silt. Canadian Geotechnical Journal, **48**(7): 1070-1084.

Zhu, F.Y., Bienen, B., O'Loughlin, C., Cassidy, M.J., and Morgan, N., 2019. Suction caisson foundations for offshore wind energy: cyclic response in sand and sand over clay. Geotechnique, **69**(10): 924-931.